Scalar-Based Analysis of Phase Gratings Etched in the Micro/nanofabrication Process
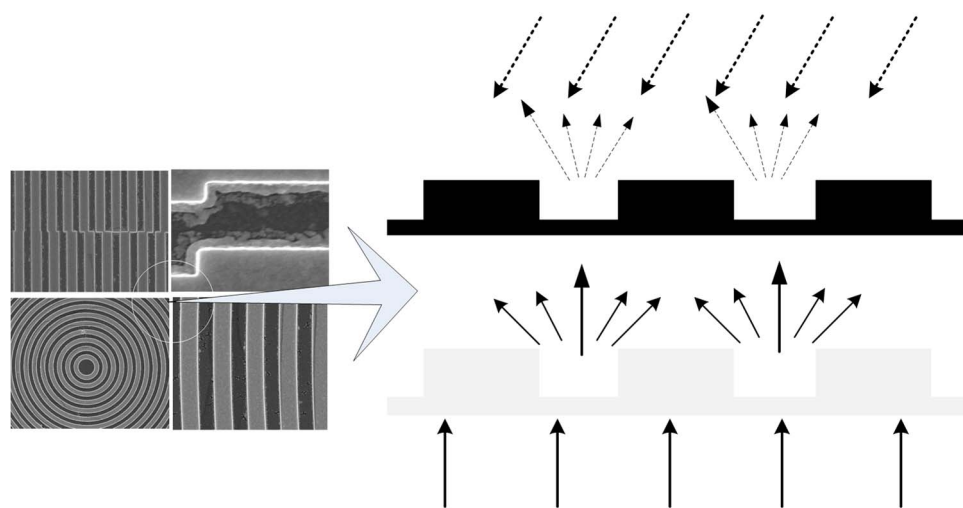
Volume 7, Number 4, August 2015

Shaolin Zhou
Yong Yang
Song Hu
Xiangmin Xu

Scalar-Based Analysis of Phase Gratings Etched in the Micro/nanofabrication Process

Shaolin Zhou,[1] **Yong Yang,**[2] **Song Hu,**[2] **and Xiangmin Xu**[1]

[1]School of Electronic and Information Engineering, South China University of Technology, Guangzhou 510640, China
[2]State Key Laboratory of Optical Technologies for Microfabrication, Institute of Optics and Electronics, Chinese Academy of Sciences, Chengdu 610209, China

Abstract: The diffraction characteristics of several types of phase gratings often etched on the substrate by the micro/nanofabrication techniques are analytically explored using scalar-based analysis in this paper. The process of an incident wave being reflected or transmitted by the diffraction grating is regarded as a process of modulation, and the reflectance or transmittance can be unified as the modulation index. The mechanisms of phase modulation, amplitude modulation, and the amplitude–phase hybrid modulation in different situations are discussed. Analytical results indicate that the diffraction efficiency is directly determined by the phase difference of adjacent features, i.e., the cyclically distributed ridges and grooves that induce different phase and amplitude variations. The absolute phase grating with phase difference equivalent to π has the maximum diffraction efficiency among all types of gratings. The conclusions could, in general, provide guidance for the design and micro/nanofabrication of phase gratings for many diffraction-based applications of optical metrology or imaging.

Index Terms: Diffraction and gratings, micro/nanofabrication, phase modulation.

1. Introduction

Diffraction gratings have always been the most widely used optical components that are involved in many conventional applications and emerging technologies or phenomena, e.g., the Talbot effect [1], [2], Moiré metrology [3]–[5], spectroscopy and holography [6]–[8], as well as micro-optics [9], [10], the optical vortex [11], [12], etc. More recently, the diffraction gratings have been extensively used in a series of scenarios of micro/nanofabrication, such as Talbot lithography [13], [14]; the reference marks for wafer-mask alignment in photolithography [15], [16]; specimens for sample locating, and the tilt adjustment between master/stamp and substrate in nanoimprint and soft lithography [17], [18]. As the typical micro-optical elements, phase gratings are often produced and etched into substrates in the process of micro/nanofabrication, and these phase-modulated diffractive structures are usually micro-fabricated to be reflective due
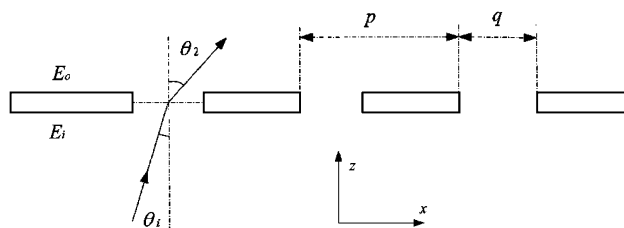
Fig. 1. Schematic of the basic modulation caused by diffractions that occur to the binary Ronchi grating at the input of a planar wave.

to high reflectivity of the substrates, e.g., the polished wafer or SiO2 substrates. Besides, the transmission type of phase gratings are also frequently etched on transparent substrate such as the quartz plate, with alternately distributed opaque metal strips and transparent quartz grooves.

Traditionally, analysis and design of such diffractive elements or periodic structures was performed in a scalar-based process for simplicity and computational efficiency, on condition that the feature sizes of such structures are much greater than the wavelength of incident light [19], [20]. Subsequently, rigorous algorithms such as the rigorous coupled-wave analysis (RCWA) are presented to obtain accurate results regardless of the feature size [21]–[23], due to the fact that sub-wavelength structures can be ultimately produced by the advanced micro/nanofabrication techniques and the scalar theory can no longer give rise to accurate results. However, the rigorous approach such as RCWA turns out to be computationally cumbersome, especially inefficient for analysis of periodic or quasi-periodic structures. Furthermore, study by Pommet also indicates that scalar theory still hold for gratings with feature size at the magnitude of five wavelengths of incident waves, and the error can be minimized close to zero especially when the fill factor of the grating equals to 0.5 [20].

Therefore, in terms of trade-off among accuracy, complexity, and computational efficiency, the scalar-based theory can still be effective guidance for design of phase gratings during micro/nanofabrication. In this paper, we analytically explore the diffraction characteristics of phase gratings often etched into substrates in a scalar-based manner, provided that the minimal feature size is no less than or around the magnitude of five wavelengths of incident wave. For both the reflection and transmission gratings, the amplitude or phase changes to the incident field is caused by discrepancies in refractive indexes and optical paths of adjacent features (ridges and grooves). And the process of reflection or transmission can also be regarded as modulation. Therefore, the modulation process was explored in a scalar-based approach to obtain the characteristics of output field and ultimately the diffraction efficiency. Further, this process can be accordingly classified into phase modulation, amplitude modulation and amplitude-phase hybrid modulation respectively. The transmittance or reflectance of phase gratings etched deep into opaque or transparent substrates is then termed as modulation coefficient. The modulation coefficients of transmission gratings with amplitude modulation, phase modulation, and amplitude-phase hybrid modulation are derived and denoted as T_{AM}, T_{PM}, and T_{APHM}. The counterparts of reflection gratings with different types of modulations are also derived and denoted as R_{AM}, R_{PM}, and R_{APHM} respectively. In particular, the binary *Ronchi* grating, the basic amplitude grating, is first introduced in the background in Section 1 with the modulation coefficient denoted by T_{Ronchi}. In final discussions, analytical results give rise to the unified expressions of modulation coefficients and diffraction efficiency, TR_{APHM} and η_{APHM} for all types of gratings, and several conclusions are drew for both the transmission and reflection gratings with different characteristics of modulations.

2. Fundamental Background

The binary Ronchi grating, shown in Fig. 1, the most frequently referred basic type of amplitude grating insofar as diffraction theory, is the basic diffraction structure and cited here for

fundamental illustration. The amplitude modulation index (i.e., transmittance) is usually expressed as

$$T_{Ronchi} = \sum_{n=-\infty}^{+\infty} rect\left(\frac{x-np}{q}\right) = \sum_{n=-\infty}^{+\infty} a_n \exp\left(i2\pi n\frac{x}{p}\right) \tag{1}$$

where, $a_n = \beta \mathrm{sinc}\,(\beta n)$, $\beta = q/p$ is the fill factor (FF) of the grating, and $rect(x/q)$ denotes the rectangular function with width q, namely

$$rect\left(\frac{x}{q}\right) = \begin{cases} 1; & |x| < q \\ 0; & \text{otherwise.} \end{cases}$$

As indicated by the Fourier Optics, the field behind the grating illuminated by a planar wave can be treated as a combination of all diffracted waves with different spatial frequencies (or wave vectors). Namely, at the incidence of a planar wave from an angle of θ_i, shown in Fig. 1, the output field E_o behind the grating can be expressed as

$$E_o = E_i \cdot T_{Ronchi} = \sum_{n=-\infty}^{+\infty} a_n \exp\left(i\vec{k}_o^n \cdot \vec{r}\right). \tag{2}$$

Therefore, $\vec{r} = (x, y, 0)$ denotes the output plane behind the grating, $\vec{k}_o^n = \vec{k}_i + \vec{k}_n$ denotes wave vector of the nth output diffracted order, where

$$\vec{k}_i = \frac{2\pi}{\lambda}(\sin\theta_i, 0, \cos\theta_i) \quad \text{and} \quad \vec{k}_n = \frac{2\pi}{\lambda}(\sin\theta_n, 0, \cos\theta_n) \tag{3}$$

denote the vectors of incident wave and Ronchi grating according to the diffraction equation, $p\sin\theta_n = n\lambda$, where θ_n is diffraction angle of the nth order under normal incidence. So the frequency spectrum $S(f_x)$ of diffractive field behind the grating can be derived by Fourier transforming (2) and introducing (3):

$$S(f_x) = \mathrm{FT}(E_o) = \sum_{n=-\infty}^{+\infty} a_n \delta\left(f_x - \frac{\sin\theta_i + \sin\theta_n}{\lambda}\right). \tag{4}$$

FT(.) denotes the Fourier transform. Obviously, the amplitude a_n of the diffracted wave is not influenced by the incident angle, which just shifts the location of all orders in the spectrum of Dirac delta function, i.e. the direction of propagation. Therefore, the scalar diffraction efficiency of Ronchi grating is also independent of the incident angle, namely

$$\eta(n, \theta_i)_{Ronchi} = |a_n|^2 = \beta^2 \mathrm{sinc}^2(\beta n). \tag{5}$$

   This way, the scalar-based representation above reveals the fundamental process of modulation that can be extended to the other gratings etched on substrates by the micro/nanofabrication techniques.

3. Transmission Gratings

In micro/nanofabrication, the transmission gratings are usually etched on transparent substrates with certain amount of surface fluctuation or relief structures. The processes of modulation by the transmission relief structures include the absolute phase modulation, amplitude-phase hybrid modulation. Specifically, the grating with absolute amplitude modulation, namely the amplitude grating, can be concluded by eliminating the terms by phase modulation. Modulations by the transmission gratings are explored first in this section. The reflection gratings are treated later in an analogous way by referring to the results of transmission gratings.
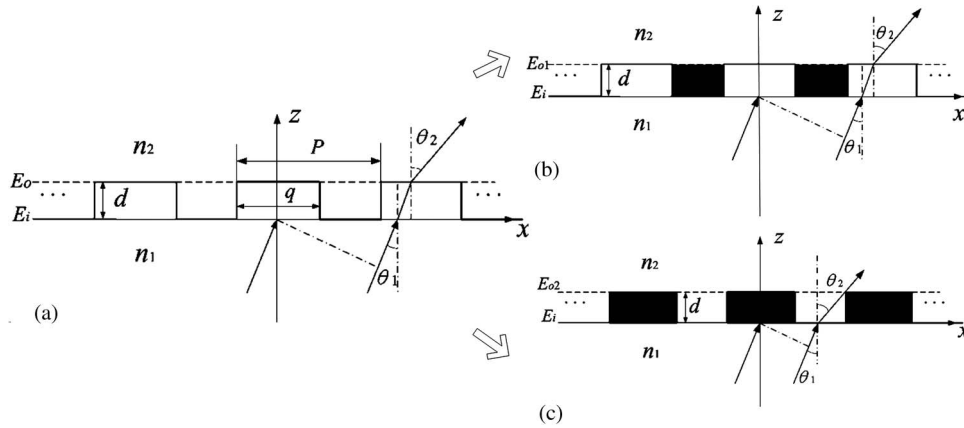
Fig. 2. (a) Transmission phase grating with periodic convex-concave interface between two media with different refraction indexes and (b), (c) two equivalently decomposed complementary structures with cyclical opaque and transparent units.

3.1. Phase Modulation

The transmission phase grating usually has a fluctuated concave-convex interface between two media with the refraction index n_1 and n_2, i.e., the cyclically and adjacently distributed ridges and grooves, shown in Fig. 2(a). When the planar wave is incident at an angle of θ_1 with respect to normal of the grating surface from the medium with refraction index n_1 and enters the other medium with refraction index n_2, diffractions and refractions occur at the convex-concave interface and result in modulation of the incident (input) field.

Take the concave (bottom) side of interface as the input plane ($z = 0$), the convex (upper) side can be then defined as the output plane of the incident wave (field). when the planar wave with unit amplitude is incident at an angle of θ_1, shown in Fig. 2, the input field in the plane of $z = 0$ can then be expressed as

$$E_i = \exp\left(i\frac{2\pi}{\lambda_0} \cdot n_1 \cdot x \sin\theta_1 \right) \tag{6}$$

The phase discrepancy emerges when the incident wave propagates in adjacent regions with different refraction indexes, i.e., the output field is phase-modulated. For simplicity, coupling between adjacent ridges and grooves is neglected, and the structure of phase grating in Fig. 2(a) is equivalently decomposed to two *Ronchi* structures, shown in Fig. 2(b) and (c). The decomposed structures are composed of adjacent regions being alternately transparent and opaque namely the simplest 0-1 mode of modulation. The black part denotes the opaque region that obstructs all waves and the white part is transparent for wave propagation. Therefore, the field in the output plane of two decomposed structures E_{o1} and E_{o2} can then be expressed as

$$E_{o1} = \exp[i\phi_1(x)]t_1(x)\gamma(\theta_1) \tag{7}$$
$$E_{o2} = \exp[i\phi_2(x)]t_2(x)\gamma(\theta_1) \tag{8}$$

where

$$\varphi_1(x) = \frac{2\pi}{\lambda_0}\left[n_1 \cdot (x - d\tan\theta_1)\sin\theta_1 + \frac{n_1 \cdot d}{\cos\theta_1} \right] = \frac{2\pi}{\lambda_0} n_1 x \sin\theta_1 + \phi_{10} \tag{9}$$

$$\varphi_2(x) = \frac{2\pi}{\lambda_0}\left[n_1 \cdot (x - d\tan\theta_2)\sin\theta_1 + \frac{n_2 \cdot d}{\cos\theta_2} \right] = \frac{2\pi}{\lambda_0} n_1 x \sin\theta_1 + \phi_{20} \tag{10}$$

denote the term of phase modulation by propagation in adjacent media with different refractive indexes $\varphi_{10} = 2\pi/\lambda_0 n_1 d \cos\theta_1$ and $\varphi_{20} = 2\pi/\lambda_0 n_2 d \cos\theta_2$ are the constant phase

factors in accordance with adjacent regions, λ_0 is the wavelength of incident wave in the air, and

$$t_1(x) = \sum_n rect\left(\frac{x - nP}{q}\right) \tag{11}$$

$$t_2(x) = 1 - t_1(x) \tag{12}$$

denote the term of amplitude modulation that is similar as the modulation coefficients of *Ronchi* grating. In addition, $\gamma(\theta_1)$ denotes the Fresnel Transmission factor (FTF), or the amplitude attenuation factor (AAF), of the interface between two media. Here, FTF $\gamma(\theta_1)$ is assumed to be consistent at both the convex and concave sides of interface. The output field of the phase grating can thus be derived as

$$E_o = E_{o1} + E_{o2} = \exp[i\phi_2(x)]\gamma(\theta_1)[\exp i(\Delta\varphi)t_1(x) + t_2(x)] \tag{13}$$

where

$$\Delta\varphi = \varphi_1 - \varphi_2 = \frac{2\pi}{\lambda_0}d \cdot (n_1\cos\theta_1 - n_2\cos\theta_2) = \varphi_{10} - \varphi_{20} \tag{14}$$

denotes the constant phase difference induced by modulation of adjacent regions. As a result, the modulation coefficients of the phase grating can be derived as

$$T_{PM}(x) = E_o/E_i = \gamma(\theta_1)\exp(i\phi_{20})[\exp i(\Delta\varphi)t_1(x) + t_2(x)] \tag{15}$$

For simplicity, the constant phase factor $\exp(i\varphi_{20})$ is neglected by shifting the original reference point. Similarly as (1) and (4), the modulation coefficient and the spectrum of output field can be simplified as

$$T_{PM}(x) = \sum_{n=-\infty}^{\infty} A_n \exp\left(i2\pi\frac{nx}{p}\right) \tag{16}$$

$$S(f_x) = FT(E_o) = \sum_{n=-\infty}^{+\infty} A_n\delta\left[f_x - \left(\frac{n_1\sin\theta_1}{\lambda_0} + \frac{n_2\sin\theta_n}{\lambda_0}\right)\right] \tag{17}$$

where

$$A_n = \begin{cases} 2j\beta\gamma(\theta_1)\sin c(\beta n)\sin\left(\frac{\Delta\varphi}{2}\right)\exp\left(j\frac{\Delta\varphi}{2}\right); (n \neq 0) \\ \gamma(\theta_1)\left[2j\beta \cdot \sin\left(\frac{\Delta\varphi}{2}\right)\exp\left(j\frac{\Delta\varphi}{2}\right) + 1\right]; (n = 0). \end{cases}$$

As a result, the diffraction efficiency can be derived as

$$\eta^T(n,\theta_1)_{PM} = |A_n|^2 = 4\beta^2\gamma^2(\theta_1)\sin c^2(\beta n)\sin^2(\Delta\varphi/2) \tag{18}$$

3.2. Amplitude-Phase Hybrid Modulation

Practically, transmission phase gratings etched on the transparent quartz substrates in the micro/nanofabrication process may have different amplitude attenuation factors for adjacent regions of media with different refractive indexes, i.e., the transparent regions in Fig. 2(b) and (c). In this situation, the incident wave (field) is modulated in a complicated hybrid way: *both phase and amplitude.* For simplicity, the transmission phase grating is assumed to have different but consistent AAF, γ_1 and γ_2, within the adjacent regions of media (ridges and grooves). Taken into account the amplitude attenuation as well as the phase modulation that occurs

concurrently the output field and the amplitude-phase hybrid modulation coefficient can be derived as

$$E_o = E_{o1} + E_{o2} = \gamma_1 \exp[i\varphi_2(x)] \cdot [\exp(i\Delta\varphi)t_1(x) + \alpha t_2(x)] \tag{19}$$

$$T_{APHM}(x) = E_o/E_i = \gamma_1 \cdot [\exp(i\Delta\varphi)t_1(x) + \alpha t_2(x)] \tag{20}$$

and therefore, $\alpha = \gamma_2/\gamma_1$ is the amplitude attenuation ratio (AAR) of adjacent regions. Simplifying and expanding the modulation coefficient in (20) using Fourier series results in

$$T_{APHM}(x) = \sum_{n=-\infty}^{\infty} B_n \exp\left(i2\pi \frac{nx}{p}\right) = \sum_{n=-\infty}^{\infty} B_n \exp(i\vec{k}_n \cdot \vec{r}) \tag{21}$$

where

$$B_n = \begin{cases} \gamma_1 \cdot \beta(e^{i\Delta\varphi} - \alpha)\sin c(\beta n); & (n \neq 0) \\ \gamma_1 \cdot [\beta(e^{i\Delta\varphi} - \alpha) + \alpha]; & (n = 0). \end{cases} \tag{22}$$

Similar to that in (3), $\vec{k}_n = (2\pi/\lambda)(\sin\theta_n, 0, \cos\theta_n)$ denotes wave vector of the nth diffracted order under normal incidence, and $r = (x, y, 0)$ denote coordinate in the original output plane. As a result, the diffraction efficiency is derived as

$$\eta^T(n, \theta_1)_{APHM} = |B_n|^2 = \beta^2 \gamma_1^2 \sin c^2(\beta n)(\alpha^2 + 1 - 2\alpha \cos\Delta\varphi). \tag{23}$$

In addition, diffraction efficiency of the transmission grating with absolute amplitude modulation, namely, the amplitude grating, can be obtained by directly setting the phase difference $\Delta\varphi$ to be zero, namely

$$\eta^T(n, \theta_1)_{AM} = \beta^2 \gamma_1^2 \sin c^2(\beta n)(1 - \alpha)^2. \tag{24}$$

Specifically, the amplitude grating also becomes the binary *Ronchi* grating with the 0-1 mode amplitude modulation, when the amplitude attenuation ratio α equals to zero. In this case, diffraction efficiency expressed by (24) is found to be in well accordance with (5), except for the amplitude attenuation factor γ_1.

4. Reflection Gratings

Different from the transmission type, the reflection gratings is often etched into opaque substrates with high reflectivity in the micro/nanofabrication process. However, the reflective concave-convex interface between two media with different refractive indexes, shown in Fig. 3(a), also modulate the incident waves (fields) in a similarly hybrid way. Analogously, the reflection grating can be decomposed into two parts with different phase and amplitude modulation: individually the reflective upper and bottom regions of the interface, shown in Fig. 3(b) and (c). As a result, the modulated output field can also be expressed as a sum of two terms, $E_{o1} = \exp[i\varphi_1(x)]t_1(x)r_1$ and $E_{o2} = \exp[i\varphi_2(x)]t_2(x)r_2$ with different phase delay and AAF (or the Fresnel reflection factor) so that the modulation coefficient can be similarly derived as

$$R_{APHM} = r_1 \exp(i\varphi_2)[\exp(i\Delta\varphi)t_1(x) + \alpha t_2(x)] \tag{25}$$

where $\alpha = r_1/r_2$ is the ratio of AAF of the concave and convex reflective interface, and $\Delta\varphi$ is the difference of phase delay that can be derived from geometry in Fig. 3, namely

$$\varphi_2 = \frac{2\pi}{\lambda_0} n_2 \left(\frac{d}{\cos\theta} + \frac{d}{\cos\theta}\cos 2\theta\right) = \frac{2\pi}{\lambda_0} \cdot 2n_2 d\cos\theta \tag{26}$$

$$\Delta\varphi = -\varphi_2; \text{ (assuming that } \varphi_1 = 0). \tag{27}$$
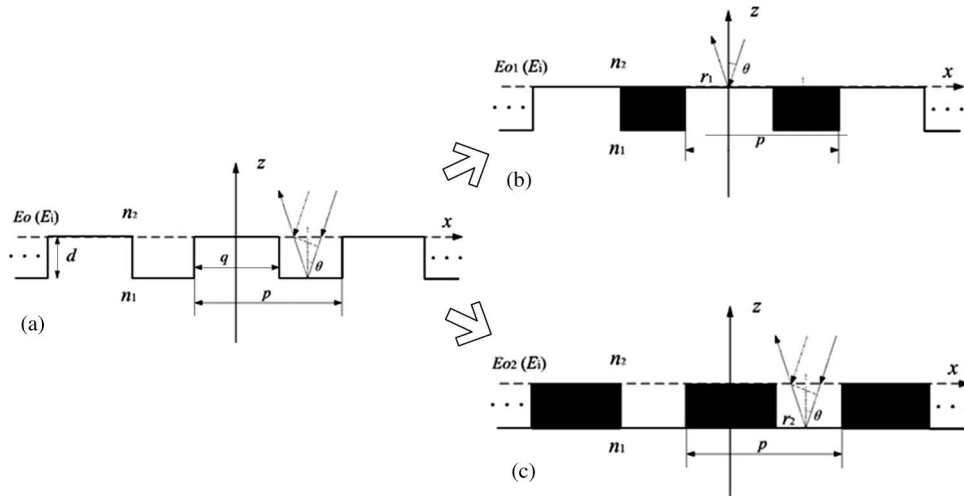
Fig. 3. (a) Schematic of incident wave modulated by the reflection phase grating and reflections that occur at the (b) upper and (c) lower surface of the transparent region of two equivalently decomposed structures.

Expanding and simplifying (25) using Fourier series result in

$$R_{APHM} = \sum_n C_n \exp\left(i2\pi\frac{x}{p}\right) = \sum_n C_n \exp(i\vec{k}_n \cdot \vec{r}) \tag{28}$$

where

$$C_n = \begin{cases} r_1 e^{i\varphi_2} \cdot \beta(e^{i\Delta\varphi} - \alpha)\sin c(\beta n); & (n \neq 0) \\ r_1 e^{i\varphi_2} \cdot \left[\beta(e^{i\Delta\varphi} - \alpha) + \alpha\right]; & (n = 0). \end{cases}$$

In the same way, the diffraction efficiency can be derived as

$$\eta^R(n, \theta_1)_{APHM} = |C_n|^2 = \beta^2 r_1^2 \sin c^2(\beta n)(\alpha^2 + 1 - 2\alpha\cos\Delta\varphi). \tag{29}$$

Correspondingly, modulation coefficient and diffraction efficiency of the reflection grating with absolute phase modulation, namely the reflection phase grating, can be obtained by setting $\alpha = 1$ in (28) and (29), namely

$$R_{PM} = \sum_n C'_n \exp\left(i2\pi\frac{x}{p}\right) = \sum_n C'_n \exp(i\vec{k}_n \cdot \vec{r}) \tag{30}$$

$$\eta^R_{PM} = 4\beta^2 r_1^2 \sin c^2(\beta n)\sin^2(\Delta\varphi/2) \tag{31}$$

where

$$C'_n = C_n|_{\alpha=1} = \begin{cases} 2i\beta r_1 \sin c(\beta n)\sin\left(\frac{\Delta\varphi}{2}\right)\exp\left(i\frac{\Delta\varphi}{2}\right); & (n \neq 0) \\ 2\beta i r_1 \sin\left(\frac{\Delta\varphi}{2}\right)\exp\left(i\frac{\Delta\varphi}{2}\right) + 1; & (n = 0). \end{cases}$$

5. Discussions and Analyses

In retrospect, rapid development of micro/nanofabrication techniques in the past decades enable accurate production of micro-optical elements including the diffraction gratings. During the process including series of steps of exposure, development and so on, the diffraction gratings are finally etched into the transparent (transmission) or opaque (reflection) substrates. Possible
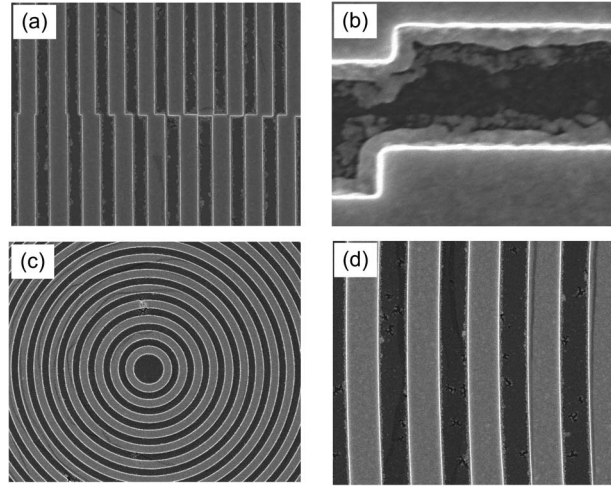
Fig. 4. Intercepted SEM images of micro-gratings fabricated by the laser-direct-writing technique as well as subsequent steps of etching and metal plating. (a) Composite phase grating composed of two grating with different periods at 2 μm and 2.2 μm. (b) Zoomed-in local regions of (a). (c) Circular gratings with period of 2 μm. (d) Zoomed-in local regions of (c).

ways of micro/nanofabrication techniques may include the conventional UV photolithography [24], X-ray lithography [25], and the E-beam lithography [26], etc., in terms of the requirements on minimal feature size. Other than that, most of those techniques need subsequent treatments like etching, lift-off and metal plating etc. In our work, the technique of E-beam lithography is adopted for fabrication of gratings with micron-level feature size, show in Fig. 4.

In conclusion, no mater what type of micro/nanofabrication techniques is used, the grating finally etched on substrate is often surface fluctuated or relieved, totally different from the conventional grating with the simplest 0-1 mode of amplitude modulation. To some extent, such structures with surface fluctuation or relief induce the functionality of phase modulation, namely the phase grating. Therefore, optimizing the structural design of phase grating is quite necessary before fabrication. The scalar-based method is used here to analytically and accurately derive/compute the diffraction characteristics, especially for those gratings with feature size no less five wavelengths of the incident light, but even for those gratings with smaller feature size, the analytical results can still provide a relative and qualitative guidance on which condition the diffraction efficiency can be maximized.

According to results in Sections 3 and 4, (21)–(23) and (28) and (29) obviously give rise to the unified expressions of the diffraction efficiency and modulation coefficient for both the transmission and reflection gratings with amplitude-phase hybrid modulation, i.e.,

$$\eta_{APHM} = \beta^2 \gamma_1^2 \sin c^2(\beta n)(\alpha^2 + 1 - 2\alpha \cos \Delta\varphi) \tag{32}$$

$$TR_{APHM} = \sum_n D_n \exp\left(i2\pi \frac{x}{p}\right) = \sum_n D_n \exp(i\vec{k}_n \cdot \vec{r}) \tag{33}$$

where

$$D_n = \begin{cases} \gamma_1 \cdot \beta(e^{i\Delta\varphi} - \alpha)\sin c(\beta n); (n \neq 0) \\ \gamma_1 \cdot \left[\beta(e^{i\Delta\varphi} - \alpha) + \alpha\right]; (n = 0) \end{cases}$$

denotes complex amplitude of the nth output diffracted wave. Therefore, α consistently denotes the ratio of AAF (amplitude ratio) for both reflection and transmission grating, γ_1 denotes the Fresnel transmission or reflection factor (i.e., the AAF) and $\Delta\varphi$ denote the phase difference induced by light propagation within the cyclically adjacent regions of media with different indexes.
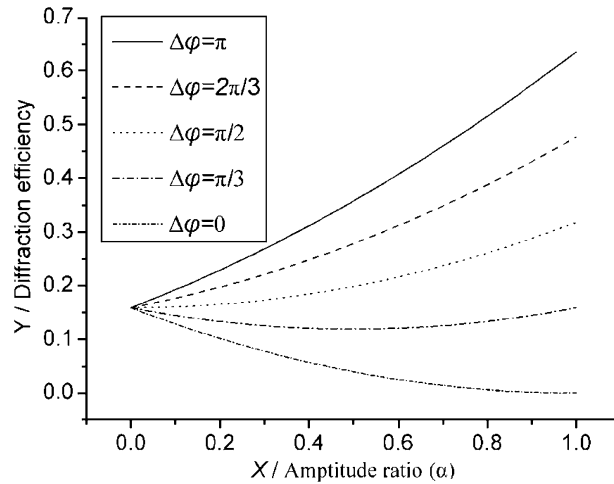
Fig. 5. Relationship between the diffraction efficiency and amplitude ratio when the fill factor $\beta = 0.5$, $\gamma_1 = 1$ is shown for the phase difference $\Delta\varphi = \pi$, $\Delta\varphi = 2\pi/3$, $\Delta\varphi = \pi/2$, $\Delta\varphi = \pi/3$, and $\Delta\varphi = 0$, respectively.

In other words, the phase gratings produced by the micro/nanofabrication techniques can be consistently treated and concluded by the final expression of (32) and (33), no matter etched on the transparent substrates for transmission gratings or the opaque substrates for reflection gratings. In addition, the constant phase factor of $\varphi_{20} = 2\pi/\lambda_0 n_2 d \cos\theta_2$ is also neglected here.

Obviously, diffraction efficiency of grating with the amplitude-phase hybrid modulation is closely associated with the phase difference $\Delta\varphi$ and the amplitude ratio α, where $\alpha \in [0\ 1]$, $\cos\Delta\varphi \in [-1\ 1]$. Take the 1st diffraction order as an example, the relationship between the diffraction efficiency and the amplitude ratio is shown in Fig. 5.

Specifically, when $\alpha = 1$, the transmission or reflection amplitude-phase hybrid gratings denoted by (32) and (33) come down to gratings with absolute phase modulation, and the diffraction efficiency is expressed as

$$\eta_{PM} = 4\beta^2\gamma_1^2 \sin c^2(\beta n) \sin \Delta\varphi/2. \tag{34}$$

When $\alpha = 0$, the amplitude-phase hybrid gratings become the binary Ronchi gratings with the amplitude attenuation factor of $\gamma 1$, and the diffraction efficiency can be simplified as

$$\eta_{Ronchi} = \beta^2\gamma_1^2 \sin c^2(\beta n). \tag{35}$$

According to analyses above and results in Fig. 5 and (32), conclusions regarding the phase gratings etched on transparent or opaque substrates can be drawn below.

a) For a constant amplitude ratio α, the diffraction efficiency increases monotonically with the increment of phase difference $\Delta\varphi$ in the range of $[0\ \pi]$, and $\Delta\varphi = \pi$ maximize the value of diffraction efficiency.

b) When $\Delta\varphi \in [\pi/2, \pi]$, diffraction efficiency increases monotonically with the increment of amplitude ratio α from 0 to 1, and $\alpha = 1$ gives rises to the maximal value (absolute phase grating) and $\alpha = 0$ the minimal value (Ronchi grating). Diffraction efficiency of grating with the amplitude-phase hybrid modulation lies between the absolute phase grating and Ronchi grating, namely

$$\eta(n, \theta_1)_{PM} \geq \eta(n, \theta_1)_{APHM} \geq \eta(n, \theta_1)_{Ronchi}. \tag{36}$$

c) When $\Delta\varphi \in [\pi/3, \pi/2]$, the diffraction efficiency of grating with amplitude-phase hybrid modulation is smaller than that of the absolute phase grating, and $\alpha = \cos\Delta\varphi$ minimize the

value of diffraction efficiency, namely

$$\eta(n, \theta_1)_{PM} \geq \eta(n, \theta_1)_{APHM} \geq \beta^2 \gamma_1^2 \sin c^2(\beta n)\sin^2 \Delta\varphi. \tag{37}$$

d) When $\Delta\varphi \in [0, \pi/3]$, $\alpha = 0$ maximize the diffraction efficiency and $\alpha = \cos\Delta\varphi$ minimize it. Under this condition, grating with the amplitude-phase hybrid modulation or absolute phase modulation has smaller diffraction efficiency than the Ronchi grating, namely

$$\eta(n, \theta_1)_{Ronchi} \geq \eta(n, \theta_1)_{APHM} \geq \beta^2 \gamma_1^2 \sin c^2(\beta n)\sin^2\Delta\varphi \tag{38}$$

and

$$\eta(n, \theta_1)_{Ronchi} \geq \eta(n, \theta_1)_{PM} \tag{39}$$

According to conclusions above, variations in the amplitude ratio α or phase difference of the cyclic adjacent regions directly change the diffraction efficiency and property of the grating, i.e., modulation type of the grating. The first conclusion indicates that increased phase difference directly leads to higher diffraction efficiency. Optimization of the diffraction efficiency is then well related to the phase difference, which can be efficiently controlled by depth of the grooves, refraction indexes of the media and the incident angle as well as wavelength in the air according to (14) and (27). Obviously, the diffraction efficiency of phase grating etched on the substrate is maximized when phase difference $\Delta\varphi = \pi$ and AAR $\alpha = 1$ (pure phase modulation), namely

$$\frac{2\pi}{\lambda_0} d(n_1 \cos\theta_1 - n_2 \cos\theta_2) = \pi$$

and the corresponding optimal depth of the grooves of grating is

$$d_{opt} = \frac{\lambda_0}{2(n_1 \cos\theta_1 - n_2 \cos\theta_2)}.$$

Specifically, when the incidence angle $\theta_1 = 0$, $d_{opt} = \lambda_0/2(n_1 - n_2)$.

6. Summary

In summary, the modulation mechanism of several types of diffraction gratings etched on opaque and transparent substrates is explored using scalar-based analysis in this paper. The diffraction efficiency and output field of phase gratings with different types of modulations can be unified by several conclusions, which indicate that optimization of these diffraction phase gratings can be realized by predetermining the phase difference and amplitude ratio of the cyclically adjacent features between two media with different refractive indexes. The analytical results could feasibly and accurately provide design criterions for many scenarios of applications, when the minimal feature size of the gratings lies at the magnitude of five wavelengths and the rigorous algorithms turn out to be computationally inefficient and extensively cumbersome. Even for diffraction grating with smaller feature size, the analytical results can still provide qualitative and relative guidance on which condition the diffraction efficiency can be maximized. Furthermore, the complex amplitude distributions in the near field can be obtained using the results of output field when the near field effect, e.g. the Talbot effect, is to be taken into consideration for different types of transmission or reflection gratings. Under many circumstances, more importance is attached to the relative intensity of diffracted orders in the far field, which can also be derived according to analytical results regarding the diffraction efficiency.

References

[1] H. Talbot, "Facts relating to optical science," *Philosoph. Mag.*, vol. 9, pp. 403–405, 1836.

[2] J. T. Winthrop and C. R. Worthington, "Theory of Fresnel images. I. Plane periodic objects in monochromatic light," *J. Opt. Soc. Amer.*, vol. 55, no. 4, pp. 373–380, 1965.

[3] I. G. O. Kafri, *The Physics of Moiré Metrology*.   New York, NY, USA: Wiley, 1989.

[4] C. A. Walker, *Handbook of Moiré Measurement*.   Bristol, PA, USA: IOP, 2004.

[5] S. Zhou *et al.*, "Fourier-based analysis of moiré fringe patterns of superposed gratings in alignment of nanolithography," *Opt. Exp.*, vol. 16, no. 11, pp. 7869–7880, May 2008.

[6] M. Verbist, W. Bogaerts, and D. Van Thourhout, "Design of weak 1-D Bragg grating filters in SOI waveguides using volume holography techniques," *J. Lightw. Technol.*, vol. 32, no. 10, pp. 1915–1920, May 2014.

[7] B. L. Volodin, J. Eichenberger, and K. Sayano, "High-resolution compact imaging holographic Bragg grating spectrometer," in *Proc. Summaries Papers presented at CLEO*, 1998, pp. 401–402.

[8] C. Peroz *et al.*, "High-resolution spectrometer-on-chip based on digital planar holography," *IEEE Photon. J.*, vol. 3, no. 5, pp. 888–896, Oct. 2011.

[9] N. Gao, H. Li, X. Zhu, Y. Hua, and C. Xie, "Quasi-periodic gratings: Diffraction orders accelerate along curves," *Opt. Lett.*, vol. 38, no. 15, pp. 2829–2831, Aug. 1, 2013.

[10] D. R. T. Brunner, B. Ryba, and J. Maass, "Tailored micro-optical and sub-wavelength structures: Manufacturing and application," in *Proc. PHOTONICS*, 2012, pp. 1–3.

[11] Y. Zhang, N. Gao, and C. Xie, "Using circular Dammann gratings to produce impulse optic vortex rings," *Appl. Phys. Lett.*, vol. 100, no. 4, 2012, Art. ID. 041107.

[12] Z. Lin, A. Wang, L. Xu, and X. Zhang, "Generation of optical vortices using a helical fiber Bragg grating," *J. Lightw. Technol.*, vol. 32, no. 11, pp. 2152–2156, Jun. 2014.

[13] A. Isoyan *et al.*, "Talbot lithography: Self-imaging of complex structures," *J. Vac. Sci. Technol. B, Microelectron. Process. Phenom.*, vol. 27, pp. 2931–2937, 2009.

[14] H. H. Solak, C. Dais, and F. Clube, "Displacement Talbot lithography: A new method for high-resolution patterning of large areas," *Opt. Exp.*, vol. 19, no. 11, pp. 10 686–10 691, May 23, 2011.

[15] W. Chen, W. Yan, S. Hu, Y. Yang, and S. Zhou, "Extended dual-grating alignment method for optical projection lithography," *Appl. Opt.*, vol. 49, no. 4, pp. 708–713, Feb. 2010.

[16] S. Zhou, S. Hu, Y. Fu, X. Xu, and J. Yang, "Moiré interferometry with high alignment resolution in proximity lithographic process," *Appl. Opt.*, vol. 53, no. 5, pp. 951–959, Feb. 2014.

[17] S. Zhou, C. Xie, Y. Yang, and S. Hu, "Moiré-based phase imaging for sensing and adjustment of in-plane twist angle," *IEEE Photon. Technol. Lett.*, vol. 25, no. 1, pp. 1847–1850, Sep. 2013.

[18] N. Li, W. Wu, and S. Y. Chou, "Sub-20-nm alignment in nanoimprint lithography using Moiré Fringe," *Nano Lett.*, vol. 6, no. 11, pp. 2626–2629, Nov. 1, 2006.

[19] D. A. Gremaux and N. C. Gallagher, "Limits of scalar diffraction theory for conducting gratings," *Appl. Opt.*, vol. 32, pp. 1948–1953, Apr. 1993.

[20] D. A. Pommet, M. G. Moharam, and E. B. Grann, "Limits of scalar diffraction theory for diffractive phase elements," *J. Opt. Soc. Amer. A, Opt. Image Sci.*, vol. 11, no. 6, pp. 1827–1834, 1994.

[21] M. G. Moharam and T. K. Gaylord, "Rigorous coupled-wave analysis of planar-grating diffraction," *J. Opt. Soc. Amer.*, vol. 71, no. 7, pp. 811–818, 1981.

[22] M. G. Moharam and T. K. Gaylord, "Rigorous coupled-wave analysis of grating diffraction-E-mode polarization and losses," *J. Opt. Soc. Amer.*, vol. 73, no. 4, pp. 451–455, 1983.

[23] M. G. Moharam and T. K. Gaylord, "Rigorous coupled-wave analysis of metallic surface-relief gratings," *J. Opt. Soc. Amer. A, Opt. Image Sci.*, vol. 3, no. 11, pp. 1780–1787, 1986.

[24] S. Zhou *et al.*, "Solvent-transfer assisted photolithography of high-density and high-aspect-ratio superhydrophobic micropillar arrays," *J. Micromech. Microeng.*, vol. 25, no. 2, 2015, Art. ID. 025005.

[25] X. Z. C. Xie, H. Li, L. Shi, and Y. Wang, "Feasibility study of hard-X-ray nanofocusing above 20 keV using compound photon sieves," *Opt. Lett.*, vol. 35, no. 23, pp. 4048–4050, Dec. 2010.

[26] K. W. Sun, S.-C. Huang, A. Kechiantz, and C.-P. Lee, "Subwavelength gratings fabricated on semiconductor substrates via E-beam lithography and lift-off method," *Opt. Quantum Electron.*, vol. 37, no. 4, pp. 425–432, Mar. 2005.